Comparison Of Position Sensorless Control Based Back-EMF Estimators in PMSM

Md. Nasir Uddin*, M M Rashid, M Rubaiyat
Department of Mechatronic Engineering
International Islamic University Malaysia
Kuala-Lumpur, Malaysia
eng.md.uddin@ieee.org, nasir.u@live.iium.edu.my

[a]Belayet Hossain, [b]S M Salam, [c]N A Nithe
Electrical & Electronics Engineering
[a]Atish Dipankar University of Science & Technology
[b]BUET, [c]I & E, Dhaka, Bangladesh
belayet_sb@yahoo.com, engnasirbd@gmail.com

***Abstract*—This research approach a study with comparison of position sensorless control schemes based on back-electromotive force (back-EMF) estimation in permanent magnet synchronous motors (PMSM). The characteristics of the estimated back-EMF signals are analyzed using various mathematical models of a PMSM. The transfer functions of the estimators, based on the extended EMF model in the rotor reference frame, are derived to show their similarity. They are then used for the analysis of the effects of both the motor parameter variations and the voltage errors due to inverter nonlinearity on the accuracy of the back-EMF estimation. The differences between a phase-locked-loop (PLL) type estimator and a Luenberger observer type estimator, generally used for extracting rotor speed and position information from estimated back-EMF signals, are also examined. An experimental study with a 250-W interior-permanent-magnet machine has been performed to validate the analyses.**

Keywords—PMSM, Back-EMF, Estimators, Sensor less, Control.

I. INTRODUCTION

Generally sensorless drives for permanent magnet synchronous motors have been widely used in many sector for their advantageous features. Example as increased reliability and reduced cost. There are proposed many sensorless methods. The methods are two types: high frequency signal injection (HFSI) [1]-[4] and back-electromotive force (back-EMF) [5]-[16]. The HFSI methods can provide relatively exact rotor position at standstill and in low-speed operating regions at the expense of audible noises and additional energy losses. The back-EMF methods acquire rotor position from the stator voltages and currents without requiring additional high frequency signal injection. This based methods are not reliable rotor position information in low-speed regions because the magnitude of the back-EMF decreases as speed decreases. However, back-EMF based sensorless methods can be successfully applied to various application where simple starting control is required such as compressors [16]. In Figure 1 shown a back-EMF estimator makes use of stator command voltages (v*), stator currents (i), and a mathematical model of the PMSM to derive the back-EMF signals. A current model-based EMF estimator was developed in [5]-[6]. However, applying this method to an interior PMSM (IPMSM) causes unstable sensorless operation, as the assumptions adopted in the model of the IPMSM are not valid in all operating ranges. To solve this problem, the extended EMF model was proposed in [7]. The extended EMF model includes saliency terms, as well as the back-EMF, so that the simplifying assumptions made to the model are not necessary. In [7] and [8], an extended EMF model in the stationary reference frame was used for sensorless control. The extended EMF model in the rotor reference frame provides the position error instead of the rotor position. However, the phase delay is negligible in this case, because the extended EMF in the rotor reference frame is a DC signal [9].

Model-based back-EMF estimators are sensitive to motor

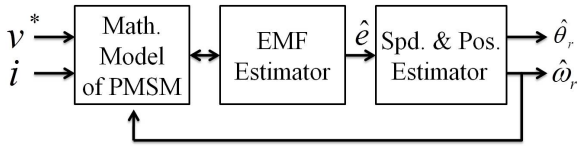

Fig.1. Functional block diagram of the back-EMF based sensor less method.

parameter variations, back-EMF harmonics, and voltage errors in the inverter [10]-[12]. The harmonics due to the nonlinearity of the inverter is the main cause of degradation of performance in back-EMF based sensorless drives at low speeds; a smaller gain for a back-EMF estimator is required to expand the lower operating range [10]. Voltage error compensation methods were used in [10]-[11] to reduce the negative effects of the inverter harmonics on a back-EMF estimator. The deviation of the motor parameters caused by magnetic saturation and thermal change also degrades the performance of back-EMF based sensorless drives. Online parameter identification is an alternative to motor parameter variations [12]-[13].

This paper evaluates three kinds of back-EMF estimators (a proportional-integral (PI) type state filter [8],

978-1-4673-9930-2/15/$31.00 ©2015 IEEE

a disturbance observer type estimator [9], [14], and a reduced-order observer [15]) based on the extended EMF model in the rotor reference frame

II. Mathematical Model of a PMSM for Back-EMF Estimation

Fig. 2 shows a space vector diagram for a PMSM [9]. The α-β and d-q frames represent the stationary and the rotor reference frames, respectively. The α axis corresponds to the magnetic axis of the u phase and the d axis is aligned with the direction of the N pole of the rotor. The γ-δ frame is an estimated frame used in sensorless vector control using the rotor reference frame. θ_r and $\hat{\theta}_r$ are the actual and estimated rotor positions, respectively.

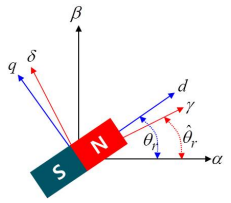

Fig.2: Vector Diagram of PMSM

A. Mathematical Model in the Stationary Reference Frame

The PMSM voltage as follows:

$$\begin{bmatrix} v_\alpha \\ v_\beta \end{bmatrix} = \begin{bmatrix} R + p(L_0 + L_1 \cos 2\theta_r) & pL_1 \sin 2\theta_r \\ pL_1 \sin 2\theta_r & R + p(L_0 - L_1 \cos 2\theta_r) \end{bmatrix} \begin{bmatrix} i_\alpha \\ i_\beta \end{bmatrix} + \omega_r \lambda_{PM} \begin{bmatrix} -\sin\theta_r \\ \cos\theta_r \end{bmatrix} \quad (1)$$

where:

v_α, v_β	stator voltage in the stationary α - β frame;
i_α, i_β	stator current in the stationary α - β frame;
R	stator resistance;
p	differential operator;
λ_{PM}	permanent magnet flux linkage;
ω_r	rotor angular velocity;
θ_r	rotor position;

$$L_0 = \frac{L_d + L_q}{2}, \quad L_1 = \frac{L_d - L_q}{2},$$

L_d and L_q are the d- and q-axes inductances.

The second term on the right-hand side of (1) is the back-EMF and it includes the rotor position information. In the case of a surface mounted PMSM (SPMSM), L_d and L_q are identical, $L_d = L_q = L_s$. So simplified eqn. (1) is follows:

$$\begin{bmatrix} v_\alpha \\ v_\beta \end{bmatrix} = \begin{bmatrix} R + pL_s & 0 \\ 0 & R + pL_s \end{bmatrix} \begin{bmatrix} i_\alpha \\ i_\beta \end{bmatrix} + \begin{bmatrix} e_\alpha \\ e_\beta \end{bmatrix} \quad (2)$$

And

$$\begin{bmatrix} e_\alpha \\ e_\beta \end{bmatrix} = \omega_r \lambda_{PM} \begin{bmatrix} -\sin\theta_r \\ \cos\theta_r \end{bmatrix}. \quad (3)$$

In SPMSM, e_α and e_β, the back-EMF signals in the stationary frame can be easily estimated using a simple estimating strategy and equation (2). However, for the IPMSM, it is difficult to construct the back-EMF observer using equation (1) owing to the unknown parameter $2\theta_r$, which is caused by the machine saliency. The extended EMF model, presented in [7], can as follows:

$$\begin{bmatrix} v_\alpha \\ v_\beta \end{bmatrix} = \begin{bmatrix} R + pL_d & \omega_r(L_d - L_q) \\ -\omega_r(L_d - L_q) & R + pL_d \end{bmatrix} \begin{bmatrix} i_\alpha \\ i_\beta \end{bmatrix} + E_{ex} \begin{bmatrix} -\sin\theta_r \\ \cos\theta_r \end{bmatrix} \quad (4)$$

where E_{ex} is the extended EMF, and is defined by (5):

$$E_{ex} = \omega_r[(L_d - L_q)i_d + \lambda_{PM}] - (L_d - L_q)(pi_q). \quad (5)$$

The second term on the right-hand side of (4) corresponds to e_α and e_β. The rotor position can be calculated as:

$$\hat{\theta}_r = -\tan^{-1}\left(\frac{\hat{e}_\alpha}{\hat{e}_\beta}\right) \quad (6)$$

Here $\hat{\theta}_r$ is the estimated rotor position, and $\hat{e}_\alpha$ and $\hat{e}_\beta$ are the back-EMF signals estimated in the stationary reference frame using (2) or (3). However, $\hat{e}_\alpha$ and $\hat{e}_\beta$ are AC signal.

B. Mathematical Model in the Rotor Reference Frame

The voltage equation as given:

$$\begin{bmatrix} v_d \\ v_q \end{bmatrix} = \begin{bmatrix} R + pL_d & -\omega_r L_q \\ \omega_r L_d & R + pL_q \end{bmatrix} \begin{bmatrix} i_d \\ i_q \end{bmatrix} + \begin{bmatrix} 0 \\ \omega_r \lambda_{PM} \end{bmatrix}. \quad (7)$$

The voltage equation of the PMSM in the γ - δ frame is:

$$\begin{bmatrix} v_\gamma \\ v_\delta \end{bmatrix} = \begin{bmatrix} R + pL_d & -\omega_r L_q \\ \omega_r L_d & R + pL_q \end{bmatrix} \begin{bmatrix} i_\gamma \\ i_\delta \end{bmatrix} + \omega_r \lambda_{PM} \begin{bmatrix} -\sin\Delta\theta \\ \cos\Delta\theta \end{bmatrix} + \mathbf{L}_a p \begin{bmatrix} i_\gamma \\ i_\delta \end{bmatrix} + \omega_r \mathbf{L}_b \begin{bmatrix} i_\gamma \\ i_\delta \end{bmatrix} + (\hat{\omega}_r - \omega_r)\mathbf{L}_c \begin{bmatrix} i_\gamma \\ i_\delta \end{bmatrix} \quad (8)$$

Here $\Delta\theta$ is the position error between the γ-δ and the d-q reference frame, $\hat{\omega}_r$ is an estimated rotor angular speed

$$\mathbf{L}_a = \begin{bmatrix} -(L_d - L_q)\sin^2\Delta\theta & (L_d - L_q)\sin\Delta\theta \cdot \cos\Delta\theta \\ (L_d - L_q)\sin\Delta\theta \cdot \cos\Delta\theta & (L_d - L_q)\sin^2\Delta\theta \end{bmatrix} \quad (9)$$

$$\mathbf{L}_b = \begin{bmatrix} -(L_d - L_q)\sin\Delta\theta \cdot \cos\Delta\theta & -(L_d - L_q)\sin^2\Delta\theta \\ -(L_d - L_q)\sin^2\Delta\theta & (L_d - L_q)\sin\Delta\theta \cdot \cos\Delta\theta \end{bmatrix} \quad (10)$$

$$\mathbf{L}_c = \begin{bmatrix} (L_d - L_q)\sin\Delta\theta \cdot \cos\Delta\theta & -L_q\cos^2\Delta\theta - L_q\sin^2\Delta\theta \\ L_d\sin^2\Delta\theta + L_q\cos^2\Delta\theta & -(L_d - L_q)\sin\Delta\theta \cdot \cos\Delta\theta \end{bmatrix}. \quad (11)$$

Eqn. (8) is complicated to be useful in building an estimator. For SPMSM, $L_d = L_q = L_s$, and thus eqn. (8) can be simplified:

$$\begin{bmatrix} v_\gamma \\ v_\delta \end{bmatrix} = \begin{bmatrix} R + pL_s & -\omega_r L_s \\ \omega_r L_s & R + pL_s \end{bmatrix} \begin{bmatrix} i_\gamma \\ i_\delta \end{bmatrix} + \omega_r \lambda_{PM} \begin{bmatrix} -\sin\Delta\theta \\ \cos\Delta\theta \end{bmatrix} + (\hat{\omega}_r - \omega_r)L_s \begin{bmatrix} -i_\delta \\ i_\gamma \end{bmatrix}. \quad (12)$$

In the γ-δ reference frame, the extended EMF can also be applied to the rotor reference frame model as follows [7], [9]:

$$\begin{bmatrix} v_\gamma \\ v_\delta \end{bmatrix} = \begin{bmatrix} R + pL_d & -\omega_r L_q \\ \omega_r L_q & R + pL_d \end{bmatrix} \begin{bmatrix} i_\gamma \\ i_\delta \end{bmatrix} + \begin{bmatrix} e_\gamma \\ e_\delta \end{bmatrix} + (\hat{\omega}_r - \omega_r)L_d \begin{bmatrix} -i_\delta \\ i_\gamma \end{bmatrix} \quad (13)$$

Here:

$$\begin{bmatrix} e_\gamma \\ e_\delta \end{bmatrix} = E_{ex} \begin{bmatrix} -\sin\Delta\theta \\ \cos\Delta\theta \end{bmatrix}. \quad (14)$$

The 2nd term on the right side of (13) is the back-EMF. The back-EMF in the γ-δ reference frame includes the rotor position error, rather than the rotor position. Under the steady-state condition, it is possible to ignore the third term on the right-hand side of (13) because the error between $\hat{\omega}_r$ and ω_r is sufficiently small and equation (13) can be simplified:

$$\begin{bmatrix} v_\gamma \\ v_\delta \end{bmatrix} = \begin{bmatrix} R + pL_d & -\omega_r L_q \\ \omega_r L_q & R + pL_d \end{bmatrix} \begin{bmatrix} i_\gamma \\ i_\delta \end{bmatrix} + \begin{bmatrix} e_\gamma \\ e_\delta \end{bmatrix}. \quad (15)$$

The estimated rotor position error $\Delta\hat{\theta}$ can be calculated:

$$\Delta\hat{\theta} = -\tan^{-1}\left(\frac{\hat{e}_\gamma}{\hat{e}_\delta}\right) \quad (16)$$

Here $\hat{e}_\gamma$ and $\hat{e}_\delta$ are the back-EMF signals estimated using (15) in the γ-δ reference frame. When using the rotor reference frame model, the estimated back-EMF signals are DC signal. On the other hand, an additional rotor position estimator is required for the rotor reference frame model because the rotor position error ($\Delta\theta$) is estimated instead of the rotor position (θ_r). In addition, the third term in (13), ignored in (15), may generate a back-EMF estimation error in the transient-state condition, where the error between $\hat{\omega}_r$ and ω_r is no longer negligible.

III. Analysis of the Back-EMF Estimator

The back-EMF signals can be estimated using either the α-β or the γ-δ reference frame model. This paper focuses on the analysis of back-EMF estimators based on the extended-EMF model in the γ-δ reference frame, because the phase delay in the back-EMF estimator is relatively small when compared to that in the α-β reference frame model.

A. Back-EMF Estimator Using PI Type State Filter

The PI type back-EMF estimator presented in [8] can also be implemented in the γ - δ reference frame model as shown in Fig. 3. In Fig. 3, $\hat{R}$, $\hat{L}_d$, and $\hat{L}_q$ are the nominal motor parameters, k_p and k_i are the proportional and integral gains of the state filter, respectively, and $\mathbf{i}_{\gamma\delta}$ is a stator current vector, which can be expressed as follows:

$$\mathbf{i}_{\gamma\delta} = i_\gamma + ji_\delta \quad (17)$$

where i_γ and i_δ are the stator currents in the γ-δ reference frame. $\hat{\mathbf{i}}_{\gamma\delta}$, $\mathbf{v}^*_{\gamma\delta}$, and $\hat{\mathbf{E}}_{\gamma\delta}$ correspond to the estimated stator current vector, the commanded voltage vector, and the estimated back-EMF vector in the γ-δ reference frame, respectively, and can be expressed in an equation similar to (17). The estimated back-EMF in Fig. 3 is given by (18)

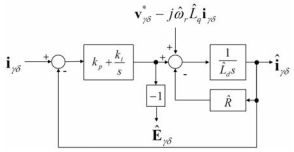

Fig. 3. Back-EMF estimator using PI type state

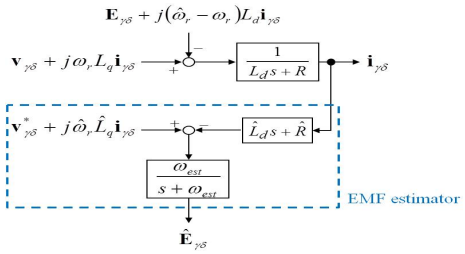

Fig. 4. Back-EMF estimator using disturbance observer.

$$\hat{\mathbf{E}}_{\gamma\delta} = \frac{(k_p s + k_i)(\hat{L}_d s + \hat{R})}{\hat{L}_d s^2 + (k_p + \hat{R})s + k_i} \times \left(\frac{\mathbf{E}_{\gamma\delta}}{L_d s + R} + \frac{\mathbf{v}^*_{\gamma\delta} - j\hat{\omega}_r\hat{L}_q\mathbf{i}_{\gamma\delta}}{\hat{L}_d s + \hat{R}} - \frac{\mathbf{v}_{\gamma\delta} - j\omega_r L_q\mathbf{i}_{\gamma\delta} - j(\hat{\omega}_r - \omega_r)L_d\mathbf{i}_{\gamma\delta}}{L_d s + R} \right) \quad (18)$$

here $\mathbf{v}_{\gamma\delta}$ is the voltage vector in the γ-δ reference frame.

The gains of the PI type back-EMF estimator:

$$k_p = \hat{L}_d\omega_{est}, k_i = \hat{R}\omega_{est} \quad (19)$$

here ω_{est} is the bandwidth of the back-EMF estimator. By substituting (19) into (18):

$$\hat{\mathbf{E}}_{\gamma\delta} = \frac{\omega_{est}}{s + \omega_{est}}\frac{\hat{L}_d s + \hat{R}}{L_d s + R}\mathbf{E}_{\gamma\delta} + \frac{\omega_{est}}{s + \omega_{est}}\left\{\mathbf{v}^*_{\gamma\delta} - j\hat{\omega}_r\hat{L}_q\mathbf{i}_{\gamma\delta} - \frac{\hat{L}_d s + \hat{R}}{L_d s + R}\left(\mathbf{v}_{\gamma\delta} - j\omega_r L_q\mathbf{i}_{\gamma\delta} - j(\hat{\omega}_r - \omega_r)L_d\mathbf{i}_{\gamma\delta}\right)\right\}. \quad (20)$$

the transfer function of the back-EMF estimator, shown in Fig. 3, is derived as follows:

$$\frac{\hat{\mathbf{E}}_{\gamma\delta}}{\mathbf{E}_{\gamma\delta}} = \frac{\omega_{est}}{s + \omega_{est}}. \quad (21)$$

From (21), it is clear that the characteristics the PI type back-EMF estimator are the same as those of a first-order low-pass filter.

B. Back-EMF Estimator Using a Disturbance Observer

Fig. 4 shows a back-EMF estimator using a disturbance observer [9]. A differential operator is included in Fig. 4. To minimize the negative effects of the differential operation, the back-EMF estimator using the disturbance observer is implemented using both a low-pass filter and a high-pass filter as follows:

$$\hat{\mathbf{E}}_{\gamma\delta} = \left(\mathbf{v}^*_{\gamma\delta} + j\hat{\omega}_r\hat{L}_q\mathbf{i}_{\gamma\delta} - \hat{R}\mathbf{i}_{\gamma\delta}\right)\left(\frac{\omega_{est}}{s + \omega_{est}}\right) - \left(\omega_{est}\hat{L}_d\mathbf{i}_{\gamma\delta}\right)\left(\frac{s}{s + \omega_{est}}\right). \quad (22)$$

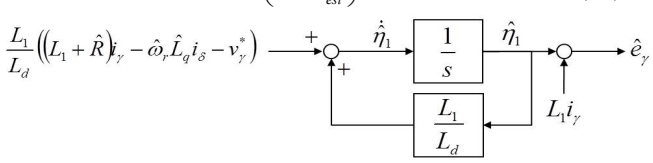

Fig. 5. Back-EMF estimator using the reduced order observer

In Fig. 6, it can bee seen that the accuracy of the back-EMF estimator is more sensitive to stator resistance

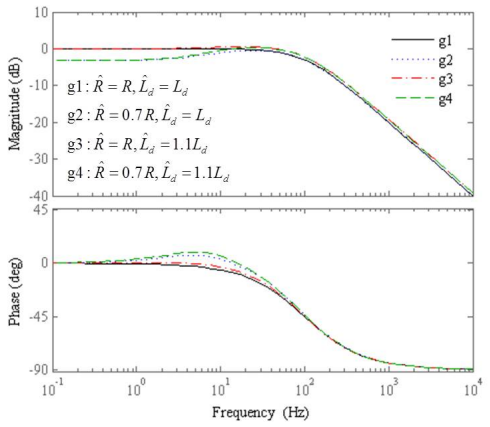

(a)

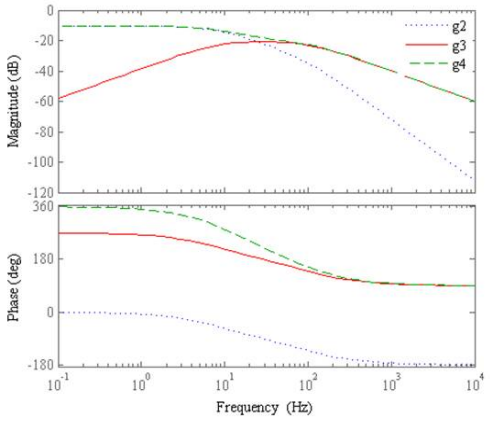

(b)

Fig. 6. Bode plots of the transfer functions (a) from the actual γ axis back-EMF to the estimated γ axis back-EMF and (b) from $v_{\gamma 1}$ to the estimated γ axis back-EMF (R = 5.8Ω, L_d = 0.11126H, ω_{est} = 100Hz).

errors than to d-axis inductance errors.

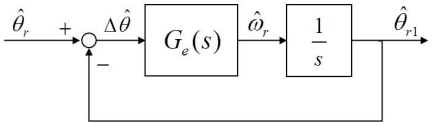

Fig. 7: PLL Type Block

IV. Speed and Position Estimators

A. PLL Type Speed and Position Estimators

The PLL type speed and position estimator shown in Fig. 7 is generally used to acquire the estimated rotor speed and position from the estimated rotor position error. The PI controller for G_e(s) in Fig. 7, which is generally used, is given as follows:

$$G_e(s) = K_{ep} + (K_{ei}/s) \tag{23}$$

and the transfer function from $\hat{\theta}_r$ to $\hat{\theta}_{r1}$ is given by (42):

$$\frac{\hat{\theta}_{r1}}{\hat{\theta}_r} = \frac{K_{ep}s + K_{ei}}{s^2 + K_{ep}s + K_{ei}}. \tag{24}$$

By assuming that the denominator of (42) is the same as the characteristic equation of the standard second-order system, K_{ep} and K_{ei} can be selected based on the damping ratio ζ and the undamped natural frequency ω_n. The transient response of the PLL type estimator can be improved by adding a double integral term into G_e(s) as follows [9]:

$$G_e(s) = K_1 + (K_2/s) + (K_3/s^2) \tag{25}$$

The transfer function from $\hat{\theta}_r$ and $\hat{\theta}_{r1}$ is given by (44):

$$\frac{\hat{\theta}_{r1}}{\hat{\theta}_r} = \frac{K_1 s^2 + K_2 s + K_3}{s^3 + K_1 s^2 + K_2 s + K_3}. \tag{26}$$

K_1, K_2, and K_3 can also be selected by using the damping ratio (ζ) and the undamped natural frequency (ω_n) [9]. Fig. 8 shows the bode plots of (42) and (44) where ζ and ω_n are set to 1 and 50 rad/s, respectively. Because the phase delay decreases, as shown in Fig. 8, when the double integral term is added, it is natural that the performance of the double integral type estimator is improved in the transient state.

B. Luenberger Observer Type Speed and Position Estimator

A Luenberger observer type speed and position estimator can also be used for the estimation of rotor speed and position, as shown in Fig. 9 [8],[17]. The transfer function of the Luenberger observer type position estimator, shown in Fig. 9, is given by (45):

$$\frac{\hat{\theta}_{r1}}{\hat{\theta}_r} = \frac{Js^3 + (B + \hat{J}K_1)s^2 + (\hat{B}K_1 + K_2)s + K_3}{\hat{J}s^3 + (\hat{B} + \hat{J}K_1)s^2 + (\hat{B}K_1 + K_2)s + K_3} \tag{27}$$

where J and B are the coefficients of the inertia and viscous friction, respectively, and $\hat{J}$ and $\hat{B}$ are the nominal parameters. The gains of the estimator in (45) can be selected such that the characteristic equation of (45) has the same roots as the followings [17]:

$$K_1 = -3\beta,\ K_2 = 3\hat{J}\beta^2,\ K_3 = -\hat{J}\beta^3 \tag{28}$$

where β is the root of the characteristic equation. To construct a Luenberger observer type speed and position estimator, the mechanical parameters J and B are required, whereas a PLL type estimator does not require the use of mechanical parameters.. Also, the PLL type estimator can filter high frequency noise included in the estimated position error, because its frequency response is the same as that of the low-pass filter, as shown in Fig. 8.

V. Experimental Results

To verify the effectiveness of the analyses of the back-EMF estimators, experiments were performed using a 250-W IPMSM coupled to a permanent-magnet DC (PMDC) load motor, as shown in Fig. 10. The parameters of the tested IPMSM are listed in Table I. The DC-links of each inverter for the tested IPMSM and the PMDC motor are connected together so that additional equipment for processing the regenerative energy from the PMDC motor is not required.

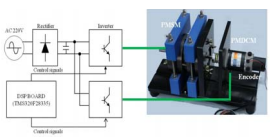

Fig.10: Experimental Set up

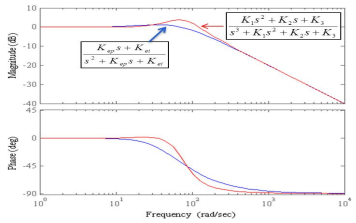

Fig. 8. Bode plots of PLL type estimators.

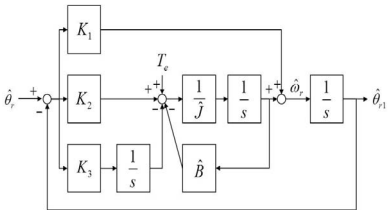

Fig. 9. Luenberger observer type speed and position estimator. [8], [17].

TABLE 1: 250-W IPMSM NOMINAL PARAMETERS

Base speed	3200 rpm
R	5.8 Ω
L_d	0.11126 H
L_q	0.165 H
λ_{PM}	0.159 Wb
Poles	6

A. The Stationary Reference Frame Model Case

To examine the characteristics of the back-EMF estimator using the stationary reference frame model, experiments were performed using the PI type back-EMF estimator presented in [8].

B. The Rotor Reference Frame Model Case

Fig. 11 and Fig. 12 show the transient and steady-state responses when the PI type back-EMF estimator using the rotor reference frame model, shown in Fig. 3, is used. The bandwidth of the back-EMF estimator is chosen to be 100 Hz. The rotor speed and position are estimated through the PLL type speed and position estimator shown in Fig. 7. The PI controller in the PLL type estimator is set to ζ =1 and ω_n=50 rad/s.

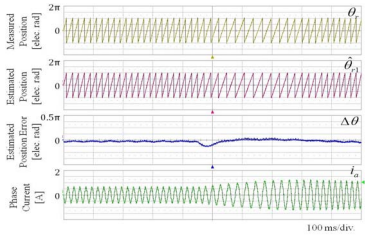

Fig. 14. Position estimated with lead-lag compensator-type PLL at rotor speed = 1000 rpm.

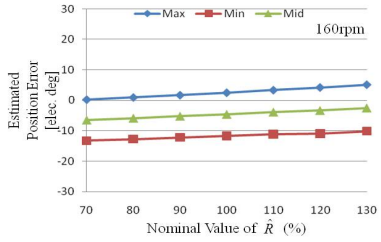

(a)

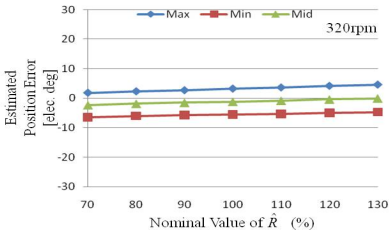

(b)

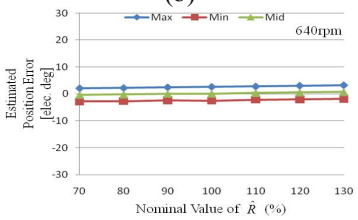

(c)

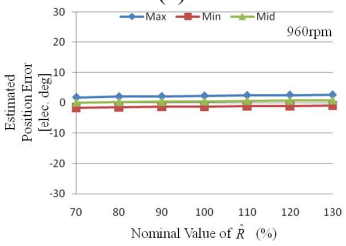

(d)

Fig. 15. Estimated position error versus nominal stator resistance variation at rated load with constant speed ((a) 5%, (b) 10%, (c) 20%, and (d) 30% of rated speed).

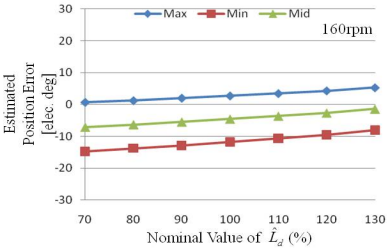

(a)

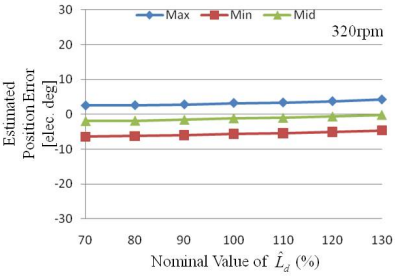

(b)

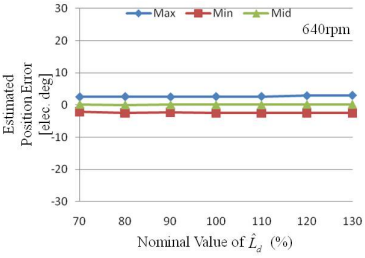

(c)

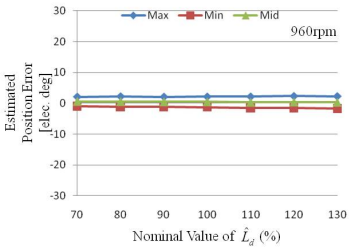

(d)

Fig. 16. Estimated position error versus nominal d-axis inductance variation at rated load with constant speed ((a) 5%, (b) 10%, (c) 20%, and (d) 30% of rated speed).

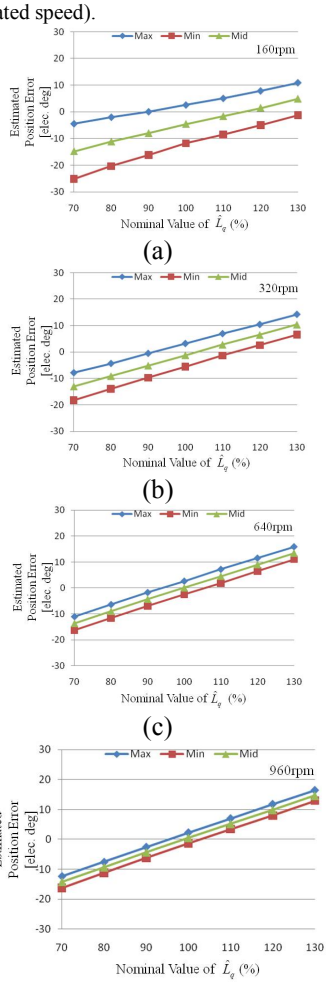

(a) (b) (c) (d)

Fig. 17. Estimated position error versus nominal q-axis inductance variation at rated load with constant speed ((a) 5%, (b) 10%, (c) 20%, and (d) 30% of rated speed).

VI. CONCLUSIONS

This paper has analyzed several back-EMF estimators for the sensorless control of a PMSM and verified the effectiveness of these analyses through experimental studies. When using the stationary reference frame model, a phase delay between the actual and the estimated back-EMF exists, because the back-EMFs in the stationary reference frame are AC signals. There are three kinds of back-EMF estimators based on the rotor reference frame model, which include the PI type, the disturbance observer type, and the reduced observer type estimator. To reduce the back-EMF estimation error at low speeds, the bandwidth of the back-EMF estimator should be decreased or a dead-time compensator can be used.

REFERENCES

[1] P. L. Jansen and R. D. Lorenz, "Transducerless position and velocity estimation in induction and salient AC machines," *IEEE Trans. Ind. Applicat.*, Vol. 31, No. 2, pp. 240-247, Mar./Apr. 1995.

[2] M. Corley and R. Lorenz, "Rotor position and velocity estimation for salient-pole permanent magnet synchronous machine at standstill and high speed," *IEEE Trans. Ind. Applicat.*, Vol. 34, No. 4, pp. 784-789, July/Aug. 1998.

[3] M. W. Degner and R. D. Lorenz, "Using multiple saliencies for the estimation of flux, position, and velocity in AC machines," *IEEE Trans. Ind. Applicat.*, Vol. 34, No. 5, pp. 1097-1104, Sep./Oct. 1998.

[4] J. Ha, K. Ide, T. Sawa, and S. Sul, "Sensorless rotor position estimation of an interior permanent-magnet motor from initial states," *IEEE Trans. Ind. Applicat.*, Vol. 39, No. 3, pp. 761-767, May/Jun. 2003.

[5] N. Matsui, T. Takeshita, and K. Yasuda, "A new sensorless drive of brushless DC motor," *in Proc. IECON '92*, pp. 430-435, 1992.

[6] N. Matsui, "Sensorless PM brushless DC motor drives," *IEEE Trans. Ind. Electron.*, Vol. 43, No. 2, pp. 300-308, Apr. 1996.

[7] Z. Chen, M. Tomita, S. Ichikawa, S. Doki, and S. Okuma, "Sensorless control of interior permanent magnet synchronous motor by estimation of an extended electromotive force," *in Conf. Rec. IEEE-IAS Annu. Meeting*, Vol. 3, pp. 1814-1819, Oct. 2000.

[8] H. Kim, M. C. Harke, and R. D. Lorenz, "Sensorless control of interior permanent-magnet machine drives with zero-phase lag position estimation," *IEEE Trans. Ind. Applicat.*, Vol. 39, No. 6, pp. 1726-1733, Nov./Dec. 2003.

[9] S. Morimoto, K. Kawamoto, M. Sanada, and Y. Takeda, "Sensorless control strategy for salient-pole PMSM based on extended EMF in rotating reference frame," *IEEE Trans. on Ind. Applicat.*, Vol. 38, No. 4, pp. 1054-1061, Jul./Aug. 2002.

[10] R. W. Hejny, and R. D. Lorenz, "Evaluating the practical low-speed limits for back-EMF tracking-based sensorless speed control using drive stiffness as a key metric," *IEEE Trans. on Ind. Applicat.*, vol. 47, pp. 1337–1343, May/Jun. 2011.

[11] Y. Inoue, Y. Kawaguchi, S. Morimoto, and M. Sanada, "Performance improvement of sensorless IPMSM drives in a low-speed region using online parameter identification," *IEEE Trans. Ind. Applicat.*, Vol. 47, No. 2, pp. 798-804, Mar./Apr. 2011.

[12] Y. Inoue, K. Yamada, S. Morimoto, and M. Sanada, "Effectiveness of voltage error compensation and parameter identification for model based sensorless control of IPMSM," *IEEE Trans. Ind. Applicat.,* Vol. 45, No. 1, pp. 213-221, Jan./Feb. 2009.

[13] S. Ichikawa, M. Tomita, S. Doki, and S. Okuma, "Sensorless control of synchronous reluctance motors based on extended EMF models considering magnetic saturation with online parameter identification," *IEEE Trans. Ind. Applicat..*, Vol. 42, No. 5, pp. 1264-1274, Sep./Oct. 2006.

[14] M. Tomita, T. Senjyu, S. Doki, and S. Okuma, "New sensorless control for brushless DC motors using disturbance observers and adaptive velocity estimations," *IEEE Trans. Ind. Electron.*, Vol. 45, No. 2, pp. 274-282, Apr. 1998.

[15] J. Kim and S. Sul, "High performance PMSM drives without rotational position sensors using reduced order observer," in Conf. Rec. IEEE-IAS Annu. Meeting, pp. 75-82, 1995.

[16] B.-H. Bae, S.-K. Sul, J.-H. Kwon, and J.-S. Byeon, "Implementation of sensorless vector control for super-high-speed PMSM of turbo-compressor," *IEEE Trans. on Ind. Applicat.*, Vol. 39, No. 3, pp. 811-818, May/June, 2003.

[17] S.-K. Sul, *Control of Electric Machine Drive Systems*, John Wiley & Sons, New Jersey, 2011.